nature physics

SUPPLEMENTARY INFORMATION

https://doi.org/10.1038/s41567-020-0908-7

In the format provided by the authors and unedited.

Emergence of criticality through a cascade of delocalization transitions in quasiperiodic chains

V. Goblot[1,5], A. Štrkalj[2,5], N. Pernet[1], J. L. Lado[2,3], C. Dorow[1], A. Lemaître[1], L. Le Gratiet[1], A. Harouri[1], I. Sagnes[1], S. Ravets[1], A. Amo[4], J. Bloch[1]✉ and O. Zilberberg[2]✉

[1]Université Paris-Saclay, CNRS, Centre de Nanosciences et de Nanotechnologies, Palaiseau, France. [2]Institute for Theoretical Physics, ETH Zurich, Zürich, Switzerland. [3]Department of Applied Physics, Aalto University, Espoo, Finland. [4]Université de Lille, CNRS, UMR 8523 – PhLAM – Physique des Lasers, Atomes et Molécules, Lille, France. [5]These authors contributed equally: V. Goblot, A. Štrkalj.
✉e-mail: jacqueline.bloch@c2n.upsaclay.fr; odedz@phys.ethz.ch

Supplementary Information for

Emergence of criticality through a cascade of delocalization transitions in quasiperiodic chains

V. Goblot[1,*], A. Štrkalj[2,*], N. Pernet[1], J. L. Lado[2,3], C. Dorow[1], A. Lemaître[1], L. Le Gratiet[1], A. Harouri[1], I. Sagnes[1], S. Ravets[1], A. Amo[3], J. Bloch[1] and O. Zilberberg[2]

[1] *Université Paris-Saclay, CNRS, Centre de Nanosciences et de Nanotechnologies, 91120, Palaiseau, France*
[2] *Institute for Theoretical Physics, ETH Zürich, 8093 Zürich, Switzerland*
[3] *Department of Applied Physics, Aalto University, Espoo, Finland*
[4] *Laboratoire de Physique des Lasers Atomes et Molécules (PhLAM), 59000 Lille, France*

*These authors contributed equally to this work.

I. SELF-DUALITY ARGUMENT

A. Self-duality of the Aubry-André model

In this subsection, following the results from Ref. [1], we describe the essence of the self-duality argument and how it can be used to analyze the localization properties of the eigenmodes. The model we consider first is the tight-binding version of the Aubry-André model

$$t\left(\psi_{j+1}+\psi_{j-1}\right)+\lambda\,\cos(2\pi bj+\phi)\,\psi_j=E\,\psi_j\,, \tag{I.1}$$

where ψ_j is the wavefunction at site j, t the nearest-neighbour hopping amplitude, and λ the amplitude of the on-site potential modulation. We transform the wave functions ψ_j as

$$\psi_j=e^{i\theta j}\sum_{k=-\infty}^{k=\infty}f_k e^{ik(2\pi bj+\phi)} \tag{I.2}$$

and obtain the Fourier-transformed equation

$$\frac{\lambda}{2}\left(f_{k+1}+f_{k-1}\right)+2t\,\cos(2\pi bk+\theta)\,f_k=E\,f_k\,. \tag{I.3}$$

The two equations [(I.1) and (I.3)] are identical at the critical point, i.e. if $\lambda/t=2$. Now, we note that if we find a localized solution in Fourier space, f_k, such that $\sum_k|f_k|^2<\infty$ then, if (I.2) converges, the solution of Eq. (I.1) has the property that $\sum_n|\psi_j|^2=\infty$. In other words, the transformation (I.2) exchanges the localization properties of ψ and f eigenmodes, namely if ψ is extended, f is localized and vice-versa. In the limit when $\lambda/t\to 0$ (e.g, when $\lambda\to 0$), Eq. (I.1) describes a metallic chain with all modes ψ being extended, while when $\lambda/t\to\infty$ (e.g, when $t\to 0$), the hopping term is negligible and the eigenmodes are localized on one site. Since the same argument is applicable also for Eq. (I.3), we conclude that the transition happens exactly at critical point $\lambda/t=2$.

B. Generalized self-duality of interpolating Aubry-André-Fibonacci (IAAF) model

We apply the self-duality argument presented in the previous subsection to the IAAF model [Eq. (1) in the main text], while taking a small β expansion. We obtain the critical line λ_C/t that bounds the phase where all eigenmodes of the model are extended. First, we expand the potential modulation [cf. Eq. (2) in the main text] for small β-s and obtain

$$V(x,\beta) = \chi + \frac{1}{3}\chi\,(1-\chi^2)\,\beta^2 + \mathcal{O}(\beta^3), \tag{I.4}$$

where $\chi \equiv \cos(2\pi b x + \phi) - \cos(b\pi)$. Notice that we use the continuous version of the potential defined in the main text. To return to the discrete version, we restrict the position x to be a set of integer numbers. After expanding the potential, we approximate the quadratic β-term as

$$V_j(\beta) \approx \chi + \frac{1}{3}U\,\beta^2\,\chi, \tag{I.5}$$

where U is the spatial average over a single period of the potential modulation $V(x,\beta)$

$$U = b\int_0^{b^{-1}} \mathrm{d}x\,[1-\chi^2] = \tag{I.6}$$

$$= b\int_0^{b^{-1}} \mathrm{d}x\,[1-(\cos(2\pi b x+\phi)-\cos(b\pi))^2] = \tag{I.7}$$

$$= -\frac{1}{2}\cos(2\pi b)\,. \tag{I.8}$$

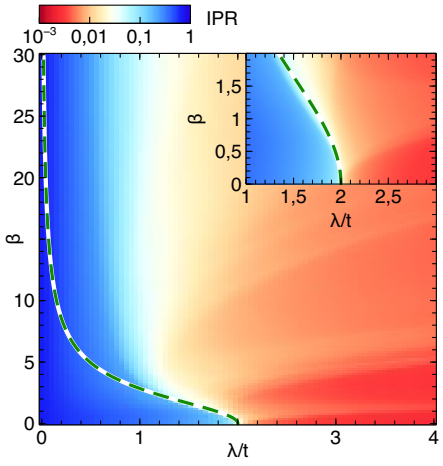

Supplementary Figure 1. **The localization phase diagram averaged over the whole spectrum.** The average localization phase diagram for all states in the spectrum obtained using the mean participation ratio [Eq. (I.12)]. The green dashed line marks the analytical result from the generalized self-duality argument (I.11). The line separates extended (blue) from localized (red) phase. The structure of localization lobes present in Fig. 1 from the main text and in Supplementary Section 3 is washed out due to the averaging over all eigenmodes of the spectrum. The size of the system is $L = 610$ sites.

In this approximation, the effective potential remains to be a cosine function incommensurate with the underlying lattice, but its amplitude is altered with the tuning parameter β. Therefore, the Hamiltonian (Eq. (1) from the main text) keeps the same shape

$$\mathcal{H}\,\psi_j = t\,(\psi_{j+1}+\psi_{j-1}) + \Lambda\,[\cos(2\pi b j+\phi)-\cos(b\pi)]\;\psi_j\,, \tag{I.9}$$

but with Λ which is now a function of β

$$\Lambda = \lambda\left(1-\frac{1}{6}\cos(2\pi b)\,\beta^2\right). \tag{I.10}$$

The self-duality point of the effective model [Eq. (I.9)] is $\Lambda/t = 2$, which implies the critical line

$$\frac{\lambda_C}{t} = \frac{2}{\left(1 - \frac{1}{6}\cos(2\pi b)\,\beta^2\right)}\,. \tag{I.11}$$

The line λ_C/t separates the extended phase from the localized one, as shown in Supplementary Fig. 1: The validity of our approximation, together with its meaning can be seen if we plot the phase diagram using the mean participation ratio defined via the inverse participation ratio (IPR) from the Eq. (3) in the main text as [3]

$$p = \left\langle IPR^{-1} \right\rangle. \tag{I.12}$$

Brackets $\langle ... \rangle$ denote the arithmetic average over all eigenmodes in the spectrum. If all the eigenmodes are localized on one site, $p \to 0$, and otherwise, for extended states, $p \to 1$.

II. LOCALIZATION-DELOCALIZATION TRANSITION WITH THOULESS'S FORMULA

In this section, the line of the first localization-delocalization transition for the lowest eigenstate is obtained analytically using Thouless's formula. The hopping term is treated as a perturbation, and thus, it is convenient to rewrite Eq. (2) in the main text as

$$\frac{t}{\lambda}\left(\psi_{j+1} + \psi_{j-1}\right) + V_j(\beta)\,\psi_j = \epsilon\,\psi_j\,, \tag{II.1}$$

where $\epsilon = E/\lambda$. For tight-binding equations of the form of Eq. (II.1), Thouless [4] established a connection between the density of states and the inverse of the localization length $l(\epsilon)$ of an eigenmode with energy ϵ

$$\frac{1}{l(\epsilon)} = \int \mathrm{d}\epsilon'\,\mathrm{DOS}(\epsilon')\,\log|\epsilon' - \epsilon| - \log\left|\frac{t}{\lambda}\right|, \tag{II.2}$$

where DOS denotes the density of states and the integral goes over the whole spectrum. The density of states for 1D quasiperiodic systems can be defined as

$$\mathrm{DOS}(\epsilon) = \mathcal{N}\left|\frac{\mathrm{d}\epsilon}{\mathrm{d}x}\right|^{-1}_{x=x(\epsilon)}, \tag{II.3}$$

where $\mathcal{N}$ is a normalization constant which assures that $\int \mathrm{DOS}(E)\,\mathrm{d}E = 1$. Notice that x is continuous variable since we have projected the states of the infinite chain to an interval $x \in [0, b^{-1}\rangle$, where b is the spatial modulation frequency of $V_j(\beta)$. The analytical calculation of the DOS for quasiperiodic systems is usually a very difficult task due to the absence of Bloch quasimomenta. However, in the case when $\lambda/t \gg 1$, it is possible to write a simple analytical expression for DOS. To do this, we set the hopping amplitude t to zero, and the energy simply follows the on-site potential

$$\epsilon = V(x, \beta). \tag{II.4}$$

Taking the derivative with respect to x and replacing $x \to x(\epsilon)$ [using the inverse of Eq. (II.4)], we obtain

$$\mathrm{DOS}(\epsilon) = \mathcal{N}\frac{\tanh\beta}{2\pi b}\frac{1}{1 - \epsilon^2\tanh^2\beta}\frac{1}{\beta\sqrt{1 - \left(\operatorname{arctanh}(\epsilon\tanh\beta) + \cos(b\pi)\right)^2}}\,. \tag{II.5}$$

Plugging the calculated density of states into Eq. (II.2), one can, in principle, obtain the localization length of every state in the spectrum.

Our goal is to obtain a closed analytical expression for the transition line λ_C/t, for the lowest-energy eigenmode, as a function of β. To this end, we expand the DOS for small β

$$\mathrm{DOS}(\epsilon) \approx \mathcal{N}\frac{1}{2\pi b}(1 + \epsilon^2\beta^2)\frac{1}{\sqrt{1 - \left(\epsilon\beta + \cos(b\pi)\right)^2}}\,, \tag{II.6}$$

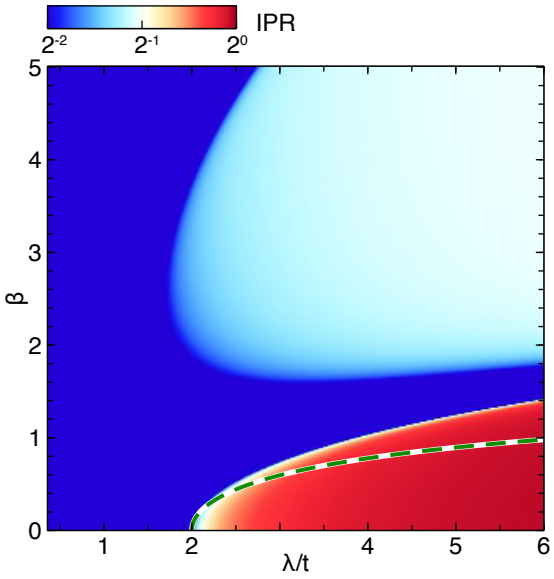

Supplementary Figure 2. **Transition line obtained by Thouless's formula.** The localization phase diagram for the lowest-energy eigenmode obtained by IPR defined in Eq. (3) of the main text. In a region colored red (white), the state is localized on one (two) site, while in blue regions state is extended. Green dashed line is an analytical prediction for the transition line where localization length diverges Eq. (II.8). The size of the system is $L = 144$ sites.

with the normalization constant taking the form $\mathcal{N} = 2b\left(1 + (\cos^2(b\pi) + \pi/2)\beta^2\right)$. Finally, we have

$$\frac{1}{l(\epsilon')} = \frac{\left(1 + (\cos^2(b\pi) + \pi/2)\beta^2\right)}{\pi} \int_{\epsilon_{\min}}^{\epsilon_{\max}} \mathrm{d}\epsilon \, (1 + \epsilon^2\beta^2) \frac{1}{\sqrt{1 - (\epsilon\beta + \cos(b\pi))^2}} \log|\epsilon - \epsilon'| - \log\left|\frac{t}{\lambda}\right| , \tag{II.7}$$

where $\epsilon_{\min} = -\tanh\left[\beta\left(1 - \cos(b\pi)\right)\right] / \tanh\beta$ and $\epsilon_{\max} = \tanh\left[\beta\left(1 + \cos(b\pi)\right)\right] / \tanh\beta$. The integral can be solved analytically for the ground state $\epsilon_G = -1 + \cos(b\pi)$ (assuming $\beta = 0$). To find the transition line, we set the localization length $l(\epsilon')$ to be infinite, and obtain the final expression

$$\log\left|\frac{\lambda_C}{t}\right| = \log 2 + \left(2\cos^2(b\pi)\log 2 + \frac{\pi}{2}\log 2 + \frac{1}{4} + \frac{1}{2}\log 2 + 2\cos(b\pi)\right)\beta^2 . \tag{II.8}$$

The critical point for the Aubry-André model, $\lambda_C = 2t$ immediately follows when we set β to zero. We show the transition line (II.8) in Supplementary Fig. 2. The line agrees well with the numerical result up to $\beta \approx 0.5$.

III. PHASE DIAGRAM FOR HIGHER-ENERGY STATES

In Supplementary Figs. 3a-f, we plot the localization phase diagram for different states in the spectrum. The same structure of lobes of localized modes, separated by narrow slivers where the modes are extended, can be observed. Furthermore, as it is shown in Supplementary Fig. 3g. all states have similar stepwise cascade of IPR when β is tuned for constant $\lambda/t \gg 2$. This indicates that all states reach criticality for $\beta \to \infty$ with the same mechanism as discussed in the main text.

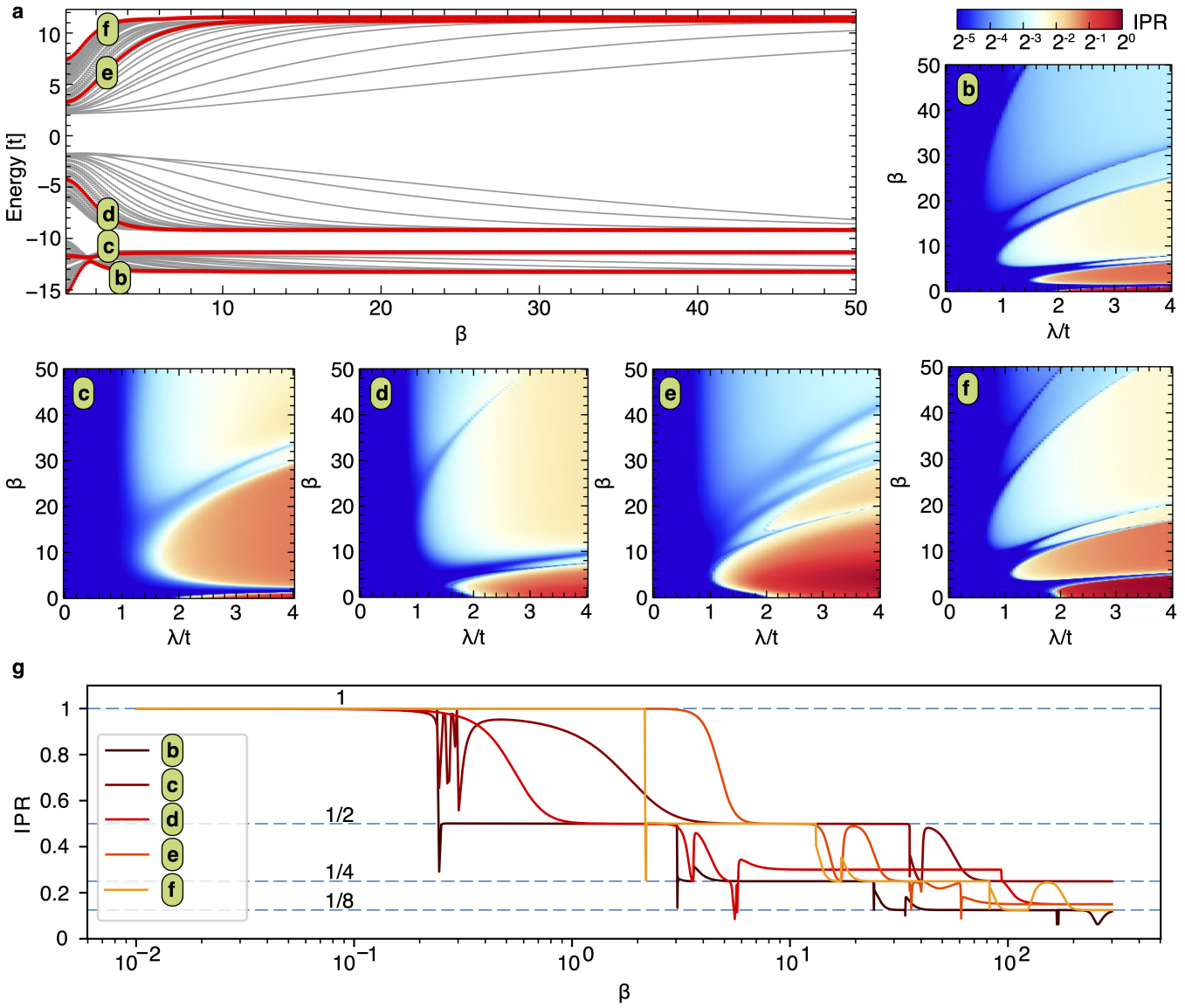

Supplementary Figure 3. **The localization phase diagram for several states in the spectrum.** **a**, The energy spectrum as a function of β for $\lambda/t = 5.5$. Several states are emphasized (red), for which we show in **b-f**, the IPR localization phase diagram [cf. Eq.(2) and Fig. 1c in the main text). **g**, IPR as a function of β for the states marked with red in **a**. All of them show similar stepwise cascade with height decreasing with a factor of 2. Here, we use $\lambda/t = 100$. A system of length $L = 144$ sites is used for all plots.

IV. TWO-SITE LOCALIZATION MECHANISM

In Supplementary Fig. 4, the mechanism behind the relocalization on 2 sites in explained. In Supplementary Fig. 4a, we see that at some point along the chain, the AA potential modulation [see Eq. (2) from the main text] arranges the onsite energies such that a nearest-neighbor pair appears close in energy. Such states strongly hybridize due to the finite hopping strength t (see Supplementary Fig. 4b). With increasing β, the marked pair of states moves towards lower energies, goes through the delocalization transition, and overtakes the role of the lowestmost energy eigenmode (see Supplementary Fig. 4c and Supplementary Video 1). The lowest energy eigenmode is then localized on two sites.

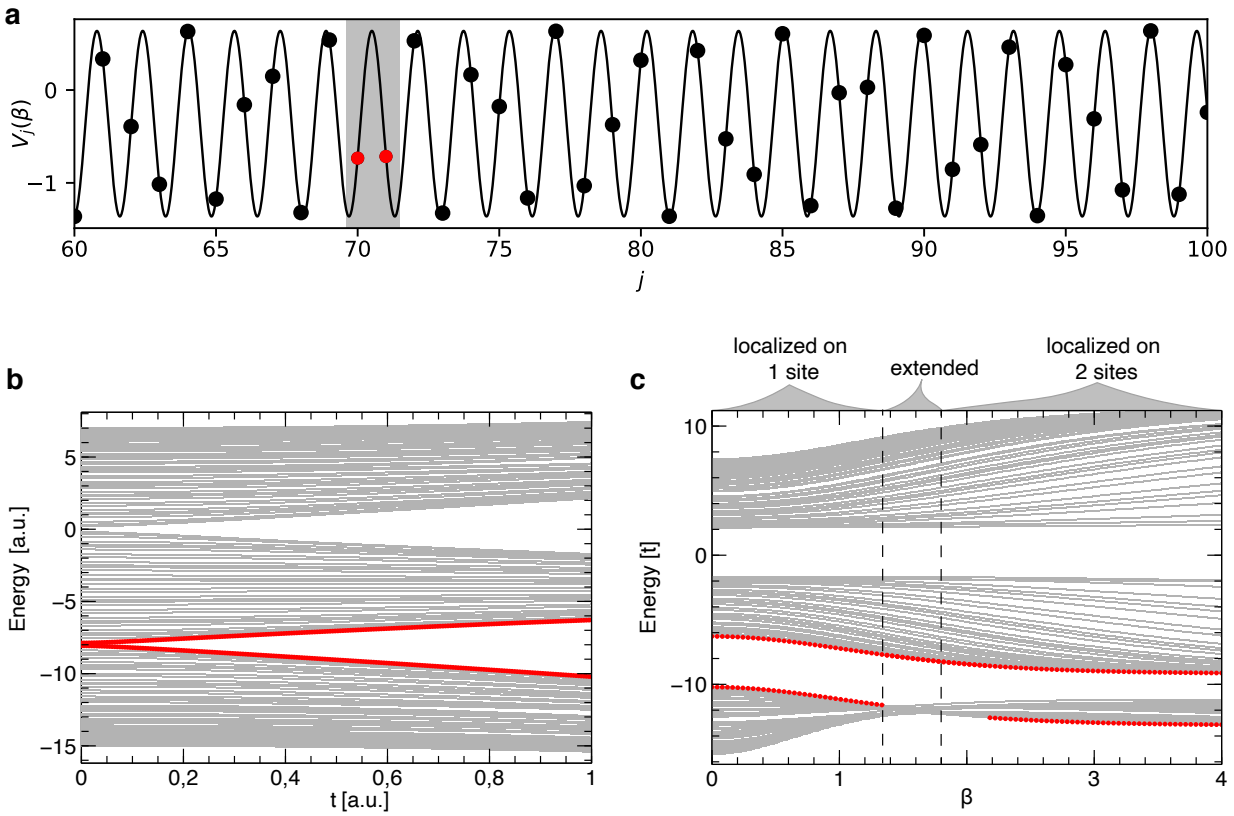

Supplementary Figure 4. **Mechanism of localization on two sites.** **a**, The potential modulation [cf. Eq. (2) in the main text] for $\beta = 0$, i.e., the AA modulation. We mark the pair of states that are both closest in energy and nearest neighbors in space, which will eventually become the lowest energy mode once β is increased. **b**, Energy spectrum of the AA model as a function of t for $\beta = 0$, $\lambda = 5.5$. With red lines, we track the aforementioned pair of states marked in **a**. For $t > 0$, a gap opens and the two marked states lie at the band edges. **c**, Energy spectrum of the IAAF model as a function of β with the marked pair of states as in **a,b**. We take $t = 1$ and the marked states are hybridized already for $\beta = 0$. By increasing β, these hybridized states are moving towards lower energies, and at some point overtake the role of the lowest energy state in the system (see also Supplementary Video 1). Vertical dashed lines mark three regions, where the lowest energy eigenmode is: localized on 1 site, extended or localized on two sites. In all plots, system has $L = 144$ sites.

A. Analytical prediction

Using the numerical analysis, we identified the mechanism of hybridization that leads to the cascade to criticality. To complement the numerical analysis, we describe this mechanism analytically for the transition of the lowest eigenmode from being localized on one site to being localized on two sites.

We start from strongly localized phase of Aubry-André model, and treat the hopping as a perturbation. First, we want to locate the energies of the pair of neighbouring states which open the lower gap in the spectrum (see states marked with red in Supplementary Figs. 4b and c) when the hopping is slowly increased. To do so, we set the hopping to zero and project all states to the reduced zone $x \in [0, b^{-1}\rangle$, which is determined by the period of a potential

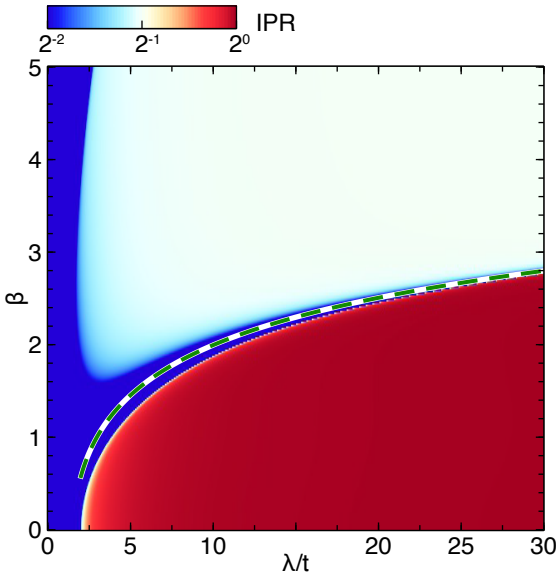

Supplementary Figure 5. **Analytical prediction for trainsition between localization on one and two sites.** The localization phase diagram for the lowest eigenmode obtained by IPR defined in Eq. (3) of the main text. In a region colored red (white), the state is localized on one (two) site, while in blue regions state is extended. Green dashed line is an analytical prediction of the transition between localization on one and two sites obtained from Eq. (IV.7). Here, the size of the system is $L = 144$ sites.

$V_j(\beta)$. In the case of an infinitely long chain, this procedure creates a continuous potential function $V(x, \beta)$ inside a reduced zone [cf. Section II]. We then search for the almost degenerate neighbouring states in the chain that satisfy the condition

$$[V(x + \delta, \beta = 0) - V(x, \beta = 0)]_{x=x'} = 0\,, \tag{IV.1}$$

where $\delta = 1$ is the spatial distance between almost degenerate neighbouring states in the chain and x' is their position in a reduced zone. The solutions of Eq. (IV.1) are

$$x'_1 = -\frac{b\pi\,\delta + \phi}{2b\pi} \tag{IV.2}$$

$$x'_2 = -\frac{b\pi\,\delta + \phi - \pi}{2b\pi}\,. \tag{IV.3}$$

The two solutions correspond to two almost degenerate neighbouring pairs of states which open the gap in a spectrum when hopping is introduced. From these two solutions it follows that the positions of the two gaps in the spectrum are

$$\epsilon_1(\beta) = V(x'_1, \beta) = -\frac{\tanh\left[\beta(\cos(b\delta\pi) + \cos(b\pi))\right]}{\tanh\beta} = 0 \tag{IV.4}$$

$$\epsilon_2(\beta) = V(x'_2, \beta) = -\frac{\tanh\left[\beta(\cos(-b\delta\pi + \pi) - \cos(b\pi))\right]}{\tanh\beta} = -\frac{\tanh\left[\beta(\cos(\pi(1-b)) - \cos(b\pi))\right]}{\tanh\beta}\,. \tag{IV.5}$$

We concentrate on the lower gap, ϵ_2 (see also Supplementary Fig. 4). The size of the gap is $2\,t/\lambda$. This means that the higher-energy state of the neighbouring pair that opened the gap is at $\epsilon = \epsilon_2 + t/\lambda$ and the lower is at $\epsilon = \epsilon_2 - t/\lambda$. From the numerical analysis in Supplementary Fig. 4c, we see that the transition from the lowest eigenmode being localized on one site to the same being localized on two sites happens when the lower-energy level of the hybridized pair passes below the previous ground state, i.e., the minimum of the potential $\min[V(j, \beta)] = \tanh\left[\beta(-1 + \cos(b\pi))\right] / \tanh\beta$. Thus, we obtain the condition for the transition to happen

$$\epsilon_2 - \frac{t}{\lambda} = \frac{\tanh\left[\beta(-1 + \cos(b\pi))\right]}{\tanh\beta}\,, \tag{IV.6}$$

from which the transition line follows

$$\frac{\lambda_C}{t} = -\left(\frac{\tanh\left[\beta(-1+\cos(b\pi))\right]}{\tanh\beta} + \frac{\tanh\left[\beta\left(\cos(\pi(1-b)) - \cos(b\pi)\right)\right]}{\tanh\beta}\right)^{-1}. \tag{IV.7}$$

We plot the transition line in Supplementary Fig. 5 and see an excellent agreement with the numerically-obtained phase diagram at high values of λ/t.

B. Supplementary Video 1 and 2

Supplementary Video 1. **The mechanism of localization on two sites** (Left panel) The grey horizontal lines mark the local density of states as a function of energy and site number j, calculated for the IAAF model [cf. Eq. (1) from the main text] at different values of β. Blue line marks the potential modulation [cf. Eq. (2) in the main text] with discrete energies (blue circles). We mark the lowest-energy eigenmode at $\beta = 0$ (blue square) and hybridized pair of nearest neighbours (red square). (Right panel) Spectrum of the IAAF model as a function of β. We mark the same states as in the left panel and with the same color code.

Supplementary Video 2. **The mechanism of localization on four sites** (Upper left panel) The grey horizontal lines mark the local density of states as a function of energy and site number j, calculated for the IAAF model [cf. Eq. (1) from the main text] at different values of β. Blue line marks the potential modulation [cf. Eq. (2) in the main text] with discrete energies (blue circles). We mark the hybridized pair of nearest neighbours (red square) and states which hybridize on four sites (green squares) at high β-s. (Upper right panel) Spectrum of the IAAF model as a function of β. We mark the same states as in the left panel and with the same color code. (Lower panel) Enlarged region from the upper right panel to see how the mode hybridized on four sites (green square) overtakes the role of the lowest-energy mode.

V. ADDITIONAL INFORMATION ON THE CONTINUUM MODEL

The eigenmodes in the continuum model are obtained numerically by diagonalization of the nearly-free particle Hamiltonian, given by Eq. (4) in the main text. The parameter values are extracted from the experiment: we use a polariton mass $m = 3 \times 10^{-5} m_e$, with m_e the free electron mass, and step length $a = 2\,\mu\text{m}$.

The definition of the IPR, given in the tight-binding model by Eq. (3) in the main text, needs to be adapted to the continuum model. In the latter case, we define the IPR of a mode $\psi(x)$ as:

$$\text{IPR} = a \int |\psi(x)|^4 \mathrm{d}x \tag{V.1}$$

The values of the IPR presented in Fig. 2a-c of the main text are computed using this definition.

VI. KINETIC ENERGY AND AUBRY-ANDRÉ LOCALIZATION IN THE CONTINUUM MODEL

Let us comment here on the relevant kinetic energy scale in the lowest band in the continuum model. In a periodic system, the characteristic kinetic energy scale is given by the recoil energy $E_R = \hbar^2 k_R^2/2m$, where $k_R = \pi/a$ is the edge of the first Brillouin zone (for a unit cell of size a). In a quasi-periodic chain, no Brillouin zone can be defined. However, in the case of the IAAF model, the gap labeling theorem predicts that gaps in the energy spectrum open at very specific wavevectors $k_{p,q}$ uniquely identified by two integers (p, q) [5]:

$$k_{p,q} = \frac{\pi}{a}(p + bq) \tag{VI.1}$$

We remind that b is the inverse of the golden mean. For our chosen value of letter size $a = 2\,\mu\text{m}$, the main gap above the lowest band opens at $k = 0.6\,\mu\text{m}^{-1}$, corresponding to $(p, q) = (-1, 1)$. In analogy with the recoil energy in a periodic system, we get a characteristic kinetic energy scale $E_R = 0.47\,\text{meV}$. Thus, in Fig. 2a of the main text, the localization transition in the AA limit is observed for $\lambda_{\text{eff}} \approx 1\,\text{meV} = 2.2 E_R$. This is consistent with the value $\lambda/t = 2$ for the AA localization transition in the tight-binding model, for which the relevant kinetic energy scale is t.

VII. TRANSVERSE PROFILE OF MODES IN DIFFERENT 1D SUBBANDS

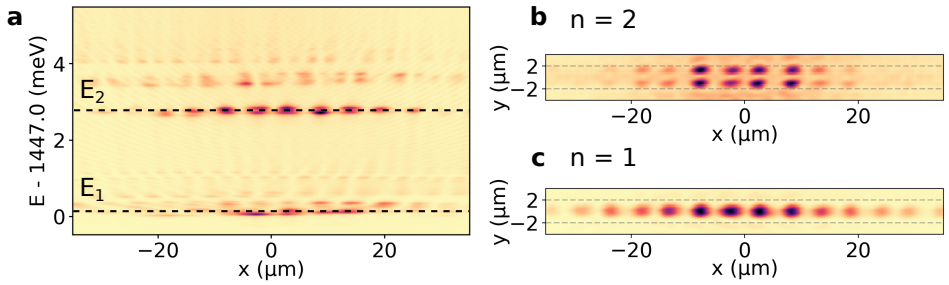

Supplementary Figure 6. **2D imaging of the eigenmodes in different subbands. a** PL intensity measured as a function of position x and energy for a wire with $\beta = 0$ and $\lambda_1 = 0.2\,\mathrm{meV}$, reproduced from Fig. 2g of the main text. **b, c** 2D image of the eigenmodes in the same wire, obtained by spectrally filtering the PL emission at energy **b**: E_2 and **c**: E_1. Dashed gray lines indicate schematically the edges of the wire (for simplicity, lateral modulations are not shown).

Real-space images of eigenmodes in the $n = 1$ and $n = 2$ subbands can be obtained by spectrally filtering the PL emission at the energy of each band. The 2D map of the emission pattern is then reconstructed from spectra such as the one shown in Supplementary Fig. 6a, measured at different values of the lateral position y on the wire. The results for both $n = 1$ and $n = 2$ subbands are presented in Supplementary Fig. 6b, c. We recognize the patterns of the $n = 1$ and $n = 2$ modes discussed in the main text: the $n = 1$ modes lateral profile has a single bright lobe, while $n = 2$ modes have the characteristic transverse profile with two bright lobes, and a zero at the center of the wire.

VIII. ESTIMATION OF THE BAND CURVATURE FOR $\beta = 1$, $\lambda_2 = 2.4\,\mathrm{meV}$

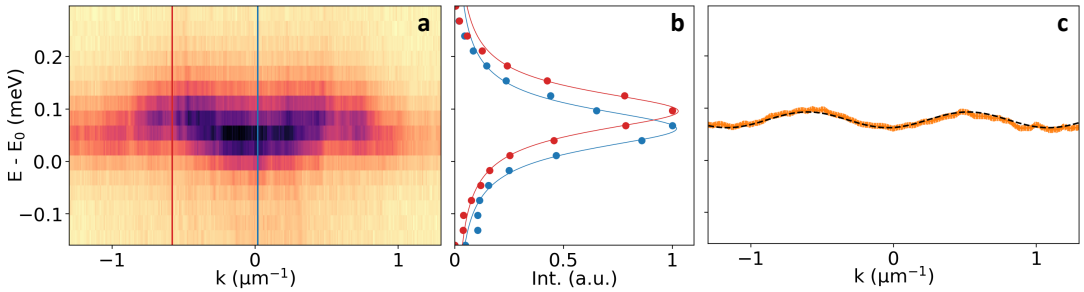

Supplementary Figure 7. **Estimation of band curvature for $\beta = 1$, $\lambda_2 = 2.4\,\mathrm{meV}$. a,** Zoom on the lowest $n = 2$ band in momentum space, reproduced from Fig. 3b of the main text. **b,** (Dots) Cut in the spectrum at two different values of k, corresponding to the solid lines in **a**, and (solid lines) respective Lorentzian fits. **c,** Energy of the band versus k, fitted by a cosine function (dashed black line) with amplitude 30 μeV.

The existence of delocalized modes in the case $\beta = 1$, $\lambda_2 = 2.4\,\mathrm{meV}$ is evidenced by the presence of a band with finite curvature, as seen in the inset of Fig. 3b(i) in the main text. In Supplementary Fig. 7, we show that in this case, the band is well fitted by a cosine function, attesting the existence of extended spatial coherence. For each k value, the energy spectrum is fitted with a Lorentzian profile with central energy $E_b(k)$, as represented in Supplementary Fig. 7b. The extracted values of $E_b(k)$ are reported in Supplementary Fig. 7c, together with the cosine fit. Note that the value of the band width extracted from the fit is approximately 30 μeV, i.e., below the polariton linewidth and comparable to the resolution of the spectrometer. This explains why, in Fig. 3d of the main text, the values of Δk measured on the first lobe remains larger (light blue) than the one measured for extended states at small λ values (dark blue).

IX. NUMERICAL SIMULATIONS FOR FIGS. 3A-D FROM THE MAIN TEXT

Supplementary Fig. 8 presents numerical calculations of the density of modes in real and reciprocal space within the continuum model, corresponding to the measured spectra presented in Figs. 3a-d of main text. An excellent agreement is found with the experiment: note, for example, how the modes localized on a single letter (down arrow) and on two letters (up arrow), at the very same location as in the experiment, and exchange energy across the delocalization-transition. The delocalization occurs when the energies of the one- and two-letter modes become resonant, i.e., between $\beta = 0.8$ and $\beta = 1$.

Note that in the derivation of the effective 1D piecewise potential $U(w_j)$ some approximations are made, that neglect corrections induced by the sharpness of the 2D confinement potential [6]. Hence our numerical simulations are computed using a value of the modulation amplitude $\lambda_{\text{eff}} = 1.8\,\text{meV}$, that is slightly smaller than the nominal value $\lambda_{\text{eff}} = 2.4\,\text{meV}$ reported in Fig. 3 of the main text. For this nominal value, the delocalization transition is observed around $\beta \approx 1.1$, as seen in Fig. 2c of the main text.

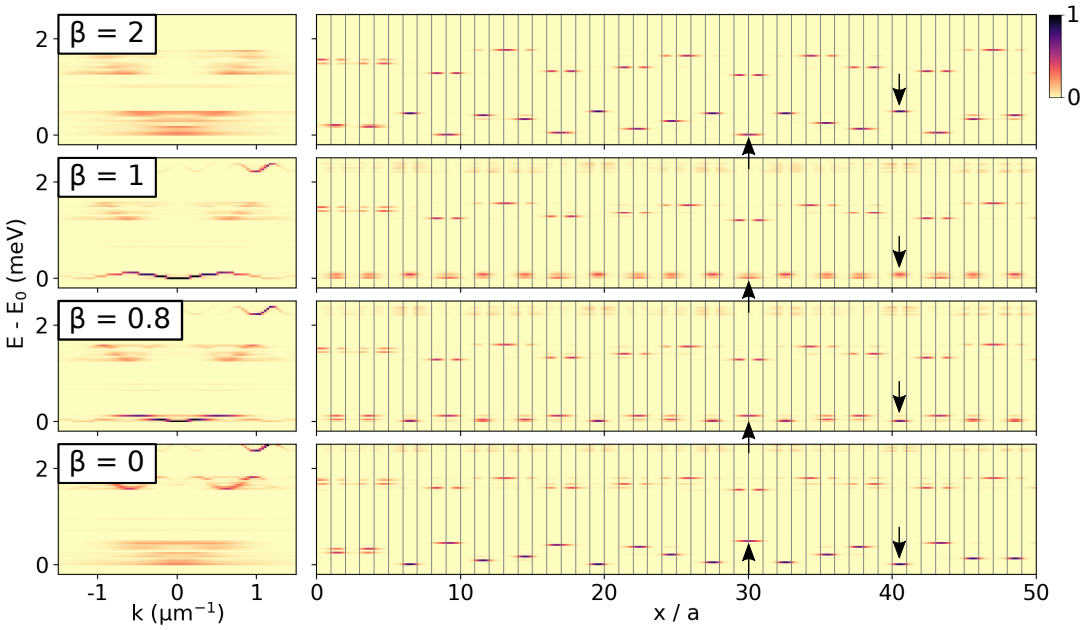

Supplementary Figure 8. **Numerical simulations corresponding to Fig. 3.a-d of main text. a-d** Calculated local density of modes, in (left) momentum- and (right) real-space, for wires with $\lambda_{\text{eff}} = 1.8\,\text{meV}$ and **a:** $\beta = 15$; **b:** $\beta = 10$; **c:** $\beta = 5$ and **d:** $\beta = 2$. Colorbar marks the normalized intensity.

X. NUMERICAL SIMULATIONS FOR THE SECOND TRANSITION

Supplementary Fig. 9 presents numerical calculations of density of modes in real and reciprocal space within the continuum model. Here we consider larger values of β to observe the second delocalization transition. As explained in the main text, we observe the formation of a band for $\beta = 10$, signature of extended eigenmodes. We also see that for $\beta < 10$, the lowest energy states are localized on 2 letters whereas they are localize on 4 letters for $\beta = 15$. This is another signature of the cascade of delocalization transitions.

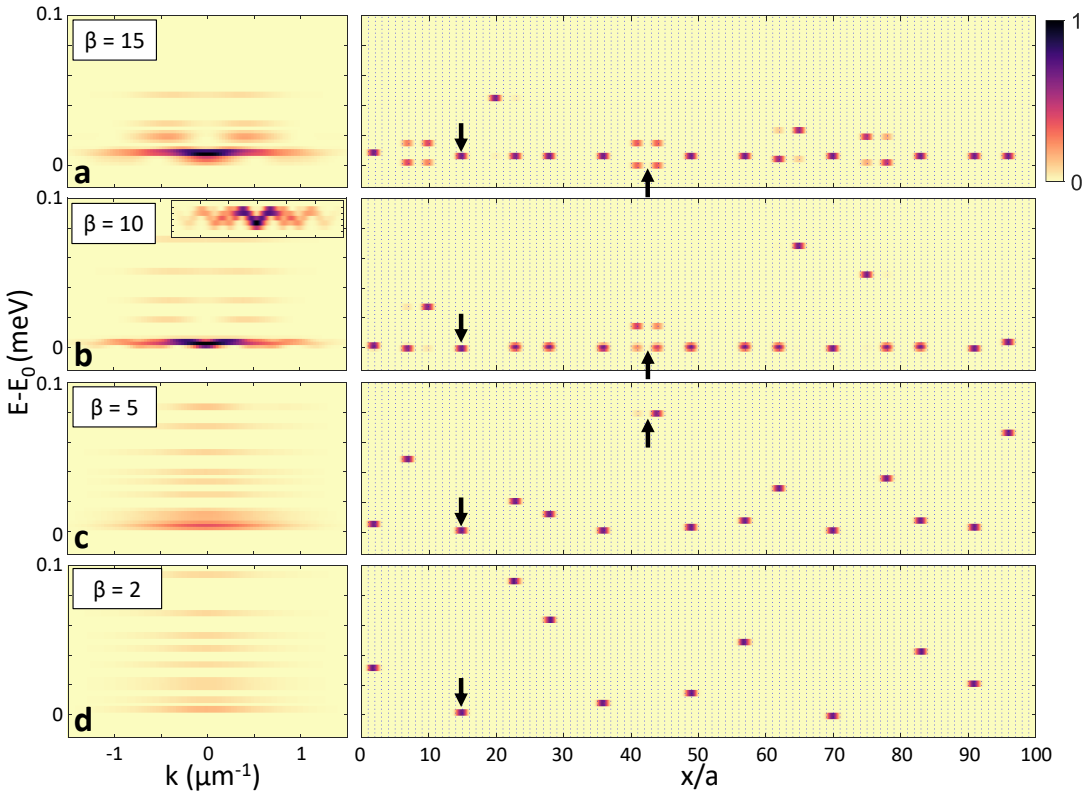

Supplementary Figure 9. **Numerical simulations showing the second transition of the cascade. a-d** Calculated local density of modes, in (left) momentum- and (right) real-space, for wires with $\lambda_{\text{eff}} = 1.8\,\text{meV}$ and **a:** $\beta =$; **b:** $\beta = 1$; **c:** $\beta = 0.8$ and **d:** $\beta = 0$. Colorbar marks the normalized intensity.

[1] S. Aubry and G. André, Ann. Israel Phys. Soc 3, 18 (1980).
[2] S. Jitomirskaya, Ann. Math. 150, 1159 (1999).
[3] S. Thiem and M. Schreiber, J. Phys.: Condens. Matter 25 075503 (2013).
[4] D. J. Thouless, J. Phys. C: Solid State Phys. 5, 77 (1972)
[5] J. Bellissard, A. Bovier, and J.-M. Ghez, Rev. Math. Phys. 4, 1 (1992).
[6] D. Tanese, E. Gurevich, F. Baboux, T. Jacqmin, A. Lemaître, E. Galopin, I. Sagnes, A. Amo, J. Bloch, and E. Akkermans, Phys. Rev. Lett. 112, 146404 (2014).